

# Scan Blindness Elimination Using Composite Defected Ground Structures and Edge-coupled Split Ring Resonators

Ming-Chun Tang<sup>1</sup>, Shaoqiu Xiao<sup>1</sup>, Chang-Jin Li<sup>2</sup>, Chaolei Wei<sup>1</sup>, and Bingzhong Wang<sup>1</sup>

<sup>1</sup> The Institute of Applied Physics

University of Electronic Science and Technology of China, Chengdu, 610054, China  
 tmc\_212@163.com, xiaoshaoqiu@uestc.edu.cn, weichaolei@126.com, bzwang@uestc.edu.cn

<sup>2</sup> Engineering and Technology College of Neijiang Normal University

Neijiang, 641112, China  
 lcj2255628@126.com

**Abstract**—A novel compact composite structure, composed of double-U shaped defected ground structure (DGS) and edge-coupled split ring resonator (E-SRR), is presented in this paper. The composite structure is integrated into microstrip array to reduce the interelement mutual coupling, with the aim to eliminate the scan blindness and improve the scanning performance. The three kinds of two-element arrays (without composite structure, with only DGS and with composite structure) are thoroughly simulated, measured, and compared. The results show that, the reduction in mutual coupling of 11 dB between elements in E-plane is obtained with the use of composite structure. It is worth mentioning that, approximately 2dB gain improvement and 2.4dB side lobe suppression are both attained, in comparison with the array with only DGSs. Finally, the scan properties of three kinds of infinite microstrip phased arrays are studied by the waveguide simulator method. The results indicate that the scan blindness in an infinite microstrip phased array can be well eliminated by virtue of the effect of the proposed composite structures, in accordance with results obtained by active patterns of the centre element in  $9 \times 5$  array.

**Index Terms** — DGS, edge-coupled SRR, scan blindness elimination.

## I. INTRODUCTION

In infinite microstrip phased arrays, scan characteristic is very poor by reason of the

occurrence of unwanted scan blindness when the interelement distance is between  $\lambda_0/2$  and  $\lambda_0$  (the operating wavelength in free space). Due to the scan blindness induced by strong surface waves, the effective methods, such as loading electromagnetic band-gap (EBG) structures and mu-negative (MNG) metamaterial between the elements, have been used extensively [1-4] to eliminate scan blindness. However, these structures witness some intrinsic defects, such as suffering complicated and high-cost designs, taking much spacing, and being of little mechanical robustness. Recently, compact DGSs of simple and low-cost design are utilized into microstrip phased array design [5] instead. Meanwhile, the etched DGS at ground plate leads to inevitable backward radiation through the DGS slot, which worsens the radiation characteristic of the whole array seriously.

To maintain the excellent capability of DGS in surface wave suppression and suppress backward radiation simultaneously, a novel compact composite structure composed of double-U shaped DGS and E-SRR is proposed to load on the infinite microstrip array to ensure high scanning performance in this paper. This paper is organized as follows: Section II firstly shows the novel double-U shaped DGS and E-SRR and analyzes their particular characteristics, respectively. Section III analyzes the influence of proposed composite structure on suppression of surface wave and backward radiation in a two-element array. Finally, the simulated results based on waveguide simulator are presented and

discussed in Section IV, demonstrating that the scan blindness is also well eliminated, in comparison with the array with only DGSs. Especially, centre active-element patterns in a  $9 \times 5$  array validate its irreplaceable performance of mutual coupling suppression and gain improvement, and the result further indicates the proposed composite structure is quite suitable for practical application because of its compact structure and good mechanical robustness.

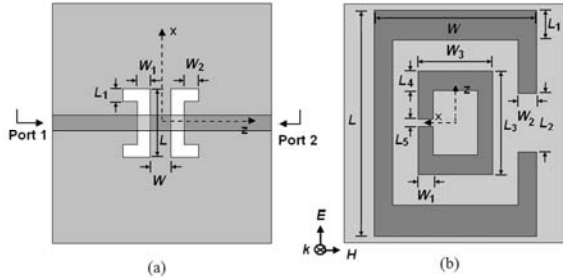


Fig. 1. Configuration of double-U shaped DGS and E-SRR. (a) Double-U Shaped DGS; The parameters:  $L = 8.7\text{mm}$ ,  $L_1 = 1.6\text{mm}$ ,  $W = 2.6\text{mm}$ ,  $W_1 = 1.6\text{mm}$ ,  $W_2 = 1.8\text{mm}$ . (The white parts indicate the slots etched in the ground plate, the grey parts indicate the ground plate, and dark grey parts indicate the microstrip transmission line.) (b) E-SRR; The parameters:  $L = 4.34\text{mm}$ ,  $L_1 = 0.585\text{mm}$ ,  $L_2 = 1.14\text{mm}$ ,  $L_3 = 2\text{mm}$ ,  $L_4 = 0.37\text{mm}$ ,  $L_5 = 0.14\text{mm}$ ,  $W = 3.11\text{mm}$ ,  $W_1 = 0.285\text{mm}$ ,  $W_2 = 0.355\text{mm}$ ,  $W_3 = 1.43\text{mm}$ , the unit cell  $x \times y \times z = 7.45\text{mm} \times 7.45\text{mm} \times 7.45\text{mm}$ . (The grey parts indicate the substrate, and the dark grey parts indicate the metal.)

## II. CHARACTERISTICS OF DOUBLE-U SHAPED DGS AND E-SRR, RESPECTIVELY

The Ansoft HFSS, an electromagnetic simulator based on the finite element method (FEM), is used to carry out all simulations in this paper. The compact double-U shaped DGS is shown in Fig. 1(a). It is etched in the ground plane under the microstrip substrate, and the substrate of 2mm thick has the dielectric constant of 10.2. A  $50\Omega$  microstrip transmission line is used to weigh the characteristics of the DGS. The DGS can be modeled by an  $L$ - $C$  resonator loaded on the transmission line. Naturally, its resonance frequency (rejection band) is also determined by  $\omega = 1/\sqrt{LC}$  according to literatures [5, 6]. Particularly, we will analyze the resonance mechanism of this type DGS and report its

performance in details in a separate paper in future. The simulation results of the DGS are shown in Fig. 2. It is observed that the -10dB stopband between 5.25GHz and 6.48GHz is obtained. Especially, the -44dB rejection level is achieved near 5.5GHz in the stopband, which demonstrate its excellent rejection performance.

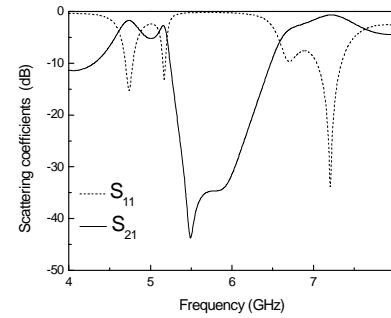
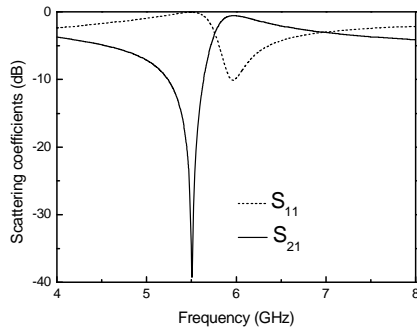
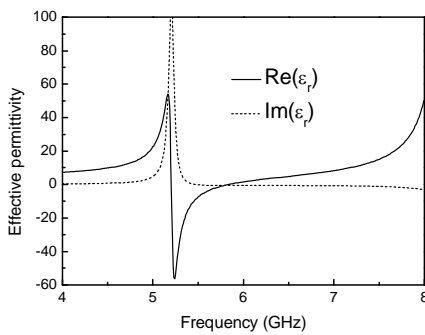


Fig. 2. Simulated scattering coefficients for configuration of double-U shaped DGS in Fig. 1(a).

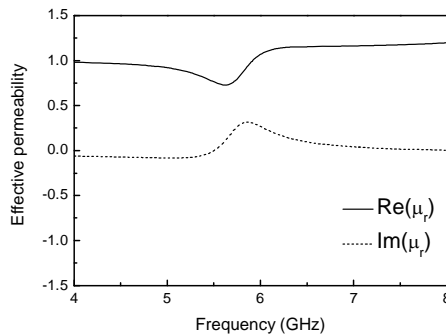
On the other hand, metamaterials have been extensively investigated recently [7-11]. Figure 1(b) gives a rectangle E-SRR structure metamaterial unit and the description of the corresponding EM environment. In this environment, the EM wave propagates perpendicularly to the E-SRR plane with the electric field  $E$  polarized parallel to the E-SRR plane and perpendicularly to the E-SRR splitting gap. Thus, the electric excitation is induced by an external electric field  $E$ , in respect that  $E$  is polarized perpendicularly to the SRR splitting gap [12-15]. Accordingly, the E-SRR can block electromagnetic wave propagating near its resonant frequency [14, 15]. It is noted that, there is no external magnetic excitation in this structure [16, 17] due to the fact that the magnetic field ( $H$ ) is polarized parallel to SRR plane. Therefore, the E-SRR can demonstrate response to the external electric field  $E$  and the block electromagnetic wave propagating near its resonant frequency [15-17]. Moreover, it is worth mentioning that, since there is no symmetry plane normal to the  $y$ -axis, magneto-electric coupling also occurs and produces magnetic response in the direction of propagation [15]. The E-SRR structure performance is also simulated and the results are shown in Fig. 3(a).



(a)



(b)



(c)

Fig. 3. Simulated scattering coefficients and retrieved effective permittivity and permeability of configuration E-SRR in Fig. 1(b); (a) simulated scattering coefficients, (b) retrieved effective permittivity, and (c) retrieved effective permeability.

The -10dB stopband between 5.25GHz and 5.64GHz is easily obtained, especially -39dB rejection level achievement near 5.4GHz, even though the dimension is much smaller than

wavelength. Moreover, the effective permittivity and permeability are extracted by the Nicolson-Ross-Weir (NRW) method [18], and the values are listed in Fig. 3(b) and (c), respectively. Obviously, there is a certain region above the resonant frequency (5.3GHz) where the E-SRR exhibits negative permittivity of a large value (in Fig. 3(b)) and positive permeability with the integer value despite of slight variations (in Fig. 3(c)), which validates its electric response. Thus, it is promising that the proposed E-SRR could provide required stopband by adjusting the metallic part dimensions in Section III.

### III. MUTUAL COUPLING REDUCTION BASED ON COMPOSITE STRUCTURE

Physically small microstrip array exhibits wide application by virtue of its excellent inherent characteristic of simple structure, light weight, small volume, low cost, and so on [4, 19]. However, mutual coupling between elements in a microstrip array, as one of the major sources of degradation in an array performance, limits its extensive application in a high-density package. Previous studies indicated that mutual coupling between the *E*-plane-coupled elements is much stronger than that between the *H*-plane-coupled elements, since stronger surface wave is excited along the *E*-plane [19-22]. Therefore, mutual coupling suppression between the *E*-plane-coupled elements is discussed in this section to demonstrate the excellent performance of the proposed composite structures.

#### A. Traditional two-element array analysis

In this section, a traditional two-element *E*-coupled microstrip array with the interelement distance between  $\lambda_0/2$  and  $\lambda_0$  is presented as an example. Figure 4 shows the layout of a two-element microstrip array with an operating frequency of 5.4GHz. The size of the two patches is  $7.7\text{mm} \times 6.7\text{mm}$ , and the interelement distance is  $37.1\text{mm}$  corresponding to  $0.65\lambda_0$  at the operating frequency. Each patch is excited on its symmetrical axis by a coaxial probe with a distance 1.05 mm away from the patch centre. A 2mm thick Rogers RT/duroid 6010/6010LM (tm) substrate ( $70\text{mm} \times 140\text{mm}$ ) with the relative permittivity  $\epsilon_r=10.2$  is selected to support the patches.

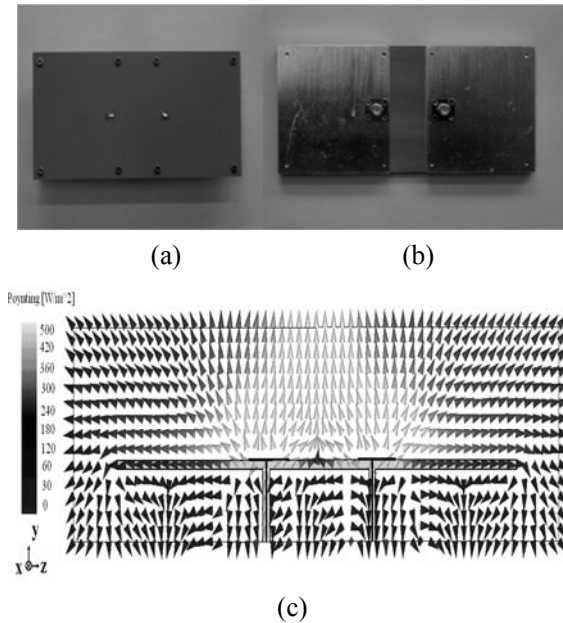


Fig. 4. Configuration of a traditional two-element array; (a) front view, (b) back view, (c) simulated Poynting vector distribution in side view, when two antenna operating.

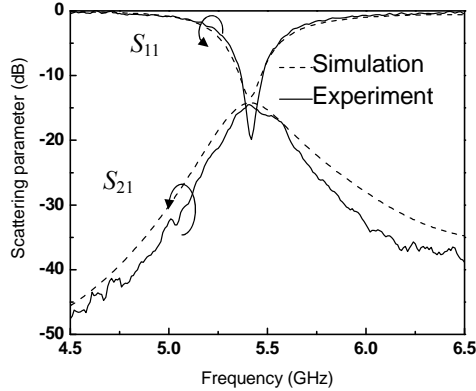


Fig. 5. Simulated and experimentally measured input matching ( $S_{11}$ ) and mutual coupling ( $S_{21}$ ) of the two patches in Fig. 4.

As shown in the previous literatures [4, 20-23], strong mutual coupling occurs between adjacent elements, on account of pronounced surface wave excited in the grounded high-permittivity substrate. The simulated and experimentally measured results are shown in Figs. 5 and 6. At the operation frequency 5.4GHz, the measured interelement

mutual coupling of -14.5dB is observed, and the gain pattern of the array is not smooth and two deep ripples appear, because of the prominent influence of the strong mutual coupling [5]. Moreover, the good front-to-back ratio of the gains of 22.3dB is measured, which validates the simulated results in Fig. 4(c), i.e., most of the EM energy is radiated in the upper free space, while the negligible back radiation is observed.

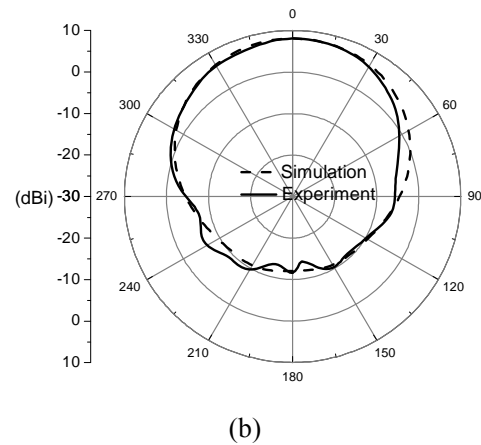
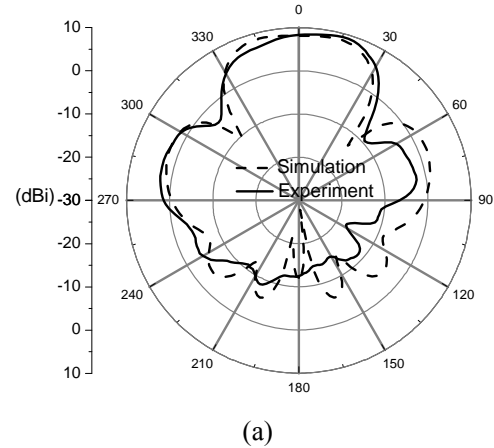


Fig. 6. Simulated and experimentally measured gain patterns of the traditional array in Fig. 4; (a) in  $E$ -plane, (b) in  $H$ -plane.

## B. Mutual coupling suppression using only DGS in two-element array

To suppress strong mutual coupling, the DGS (here, the double-U shaped DGS in Fig. 1(a) is selected as an example) is etched at the centre of the ground plate between the adjacent elements in  $E$ -plane, shown in Fig. 7. As aforementioned in Section II, the etched DGS has the inherent property

of rejection to suppress surface wave restricted within substrate [5]. When it is integrated into the array, it could bring about predominant reduction in mutual coupling for the array. Figure 8 demonstrates that mutual coupling ( $S_{21}$ ) drops drastically below -25dB around operation frequency 5.4GHz, especially -39.3dB achievement at 5.39GHz in experimental results. Obviously, it also illustrates that the DGS exhibits an excellent performance in mutual coupling reduction.

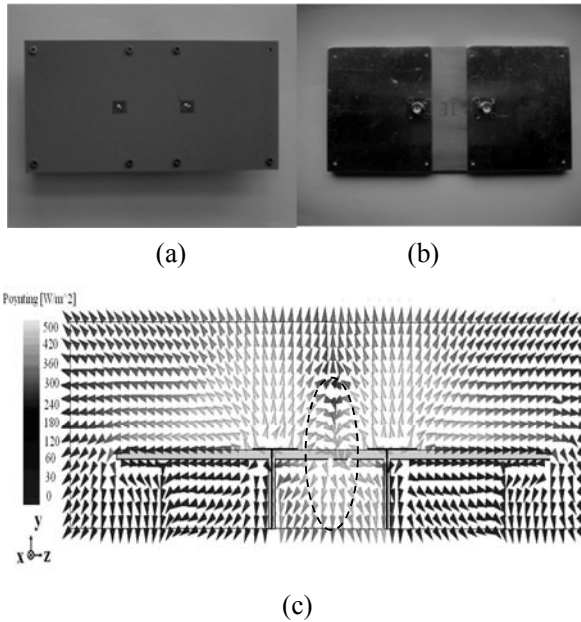


Fig. 7. Configuration of a two-element array with double-U shaped DGS; (a) front view, (b) back view, (c) simulated Poynting vector distribution in side view.

However, the etched DGS brings adverse impact on the array in Fig. 7, which incurs some EM energy, which should be radiated in the upward free space (in Fig.4(c)), leaking into the backward space through the etched DGS-slots shown in Fig. 7(c). Compared with the Poynting vector distributions in Fig. 4(c), a certain energy in the upward space turns towards the backward space (in Fig. 7(c)), which results in much decrease of upward radiation and severe increase of backward radiation. In order to further illustrate its noteworthy defect, Fig. 9 shows experimentally measured gain pattern results together with the simulated one, and they both validate the influence of the DGS on radiation performance of the array. In details, the DGS makes the radiation pattern obviously smooth because of its

performance in dramatic mutual coupling reduction. Unfortunately, this improvement is achieved at the cost of the 2.5dB peak gain reduction, 15.9dB back lobe gain increase, and 4dB front-to-back ratio of the gains achievement, in contrast with the array without DGS.

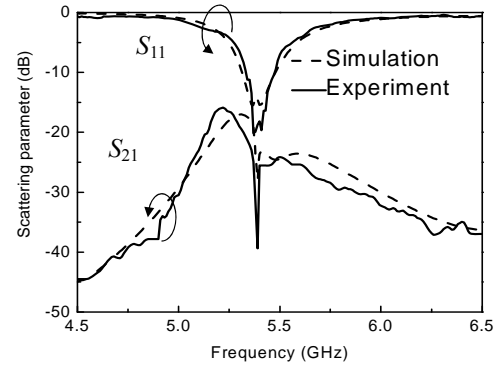
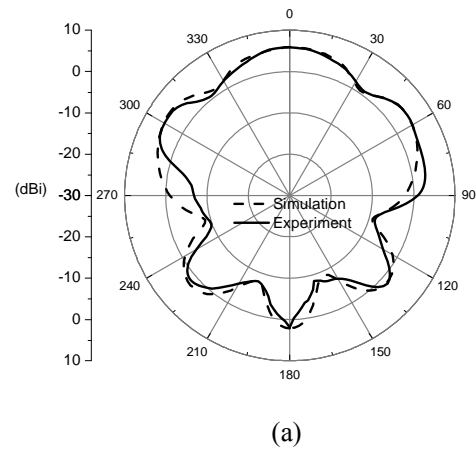


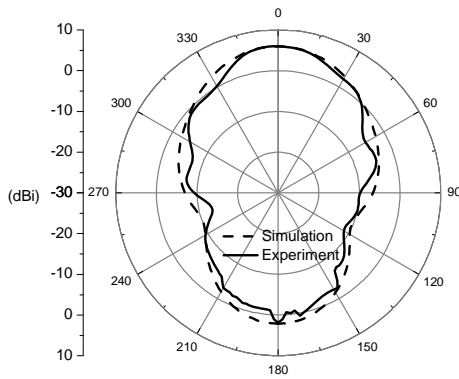
Fig. 8. Simulated and experimentally measured input matching ( $S_{11}$ ) and mutual coupling ( $S_{21}$ ) of the two patches in Fig. 7.

### C. Gain improvement using composite DGS and E-SRRs in two-element array

As it has been already mentioned in Section III(B), a certain EM wave is propagating through the slots due to the etched DGS. Furthermore, the electric field ( $E$ -field) distribution at the interface of upward free space and substrate is also simulated in Fig. 10. It is easily seen that a strong  $E$ -field region appearance above the slots (labeled in the dotted ellipse), which is predominantly polarized in the  $z$ -axis direction.



(a)



(b)

Fig. 9. Simulated and experimentally measured gain patterns of the array with DGS in Fig. 7; (a) in *E*-plane, (b) in *H*-plane.

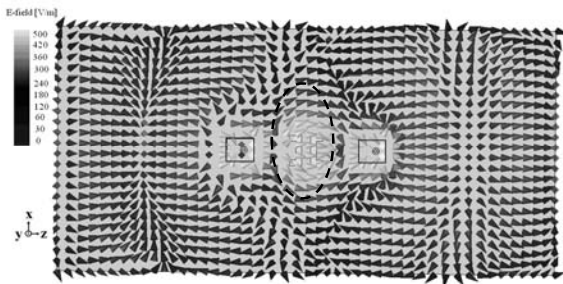
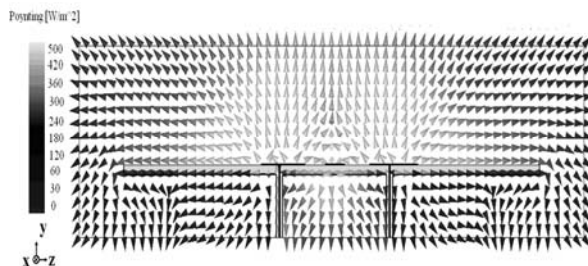


Fig. 10. Simulated *E*-field distributions in front view of the array in Fig. 7.



(a)

(b)



(c)

Fig. 11. Configuration of a two-element array with

composite double U-shaped DGS and E-SRRs; (a) front view, (b) back view, and (c) simulated poynting vector distribution in side view.

Based on the electromagnetic condition in the region of interest (in Fig. 10) well consistent with the condition shown in Fig.1(b), the three-periodic E-SRRs are proposed to be placed at the upper surface of the substrate to block the EM energy leaking into backward space [10]. It is noted that, unlike application in the free space as a semi-infinite periodic structure [23], there are only three elements etched at the substrate upper surface instead. Additionally, the DGS etched at the other side of the substrate exhibits intercoupling with the SRRs. Because of the above main factors, all the metallic part parameters of the E-SRRs given in Section II are enlarged by three quarters in order to obtain the required rejection frequency band. On the other hand, the double U-shaped DGS given in Fig. 1(a) are also adjusted in order to obtain the required rejection frequency band. To simplify the design of the DGS for the proposed array, only the length of the double slots  $L$  is optimized to  $7.4\text{mm}$  (in Figs. 11(a) and (b)). Figure 11(c) indicates that the energy leaking downwards reduces sharply compared with that in Fig. 7(c), which approves the remarkable performance of E-SRRs electric response in inhibiting EM energy from upside.

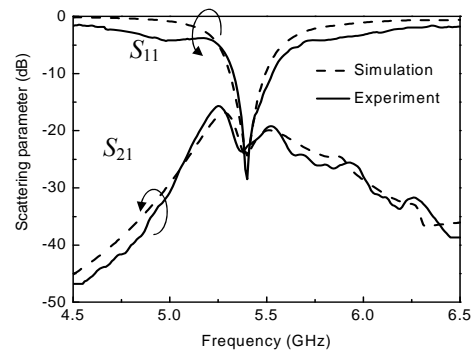
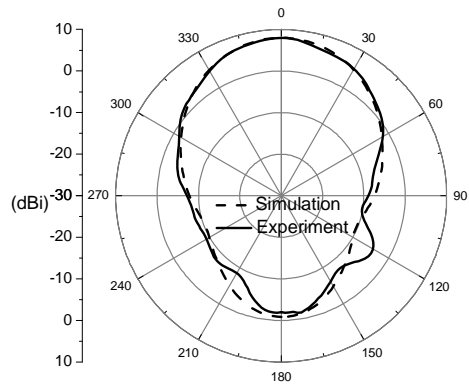


Fig. 12. Simulated and experimentally measured input matching ( $S_{11}$ ) and mutual coupling ( $S_{21}$ ) of the two patches in Fig. 11.

In the same way, the measured results together with simulated results are also shown in Figs. 12 and 13. In Fig. 12, the mutual coupling  $S_{21}$  maintains the reduction to  $-24.5\text{dB}$  around the operating frequency

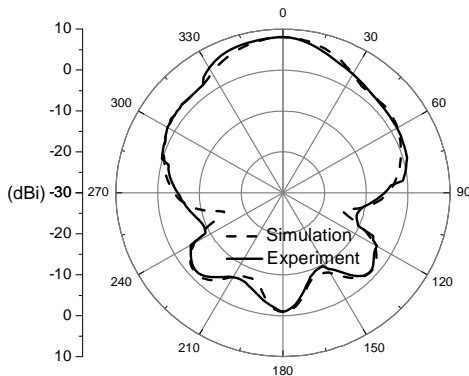
5.4GHz, and shows stabilization in its reduction. And more importantly, the gain pattern in Fig. 13 keeps smooth, the peak gain increases 2.15dB, back lobe gain drops 2.84dB and front-to-back ratio of the gains of 9.93dB, in contrast with the array with only DGS in Section III(B), which shows a close agreement with the simulated poynting vector distribution in Fig. 11(c).

Furthermore, in order to demonstrate the unique capability of the E-SRRs in improving the performance in detail, a metal sheet of the same dimensions is etched halfway between E-coupled elements instead. According to poynting vector distribution in Fig. 14, the energy propagating into backward space is neglected, by virtue of intrinsic isolation property of the metal. Figure 15 also validates the gain of main lobe and back lobe is optimized just like that in Fig. 6. However, the mutual coupling increases to -16.5dB except for a trivial variation in Fig. 16, which also damages the smoothness of the radiation pattern in *E*-plane severely shown in Fig. 15(a). That is to say, the metal above the substrate works as a surface wave “bridge” that leads the pronounced surface wave to pass across the DGS-etched region, even if the DGS possesses the characteristic of predominant suppression in mutual coupling. The above phenomenon indicates the metal sheet cannot take up the E-SRRs as an isolation wall horizontally laid at the substrate upper surface, due to its adverse impact on the mutual coupling reduction.



(b)

Fig. 13. Simulated and experimentally measured gain patterns of the array with composite structure in Fig. 11; (a) in *E*-plane, (b) in *H*-plane.



(a)

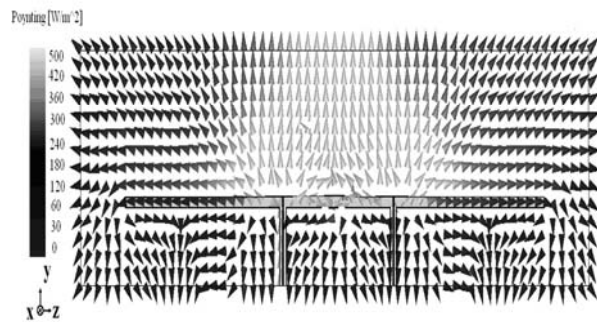
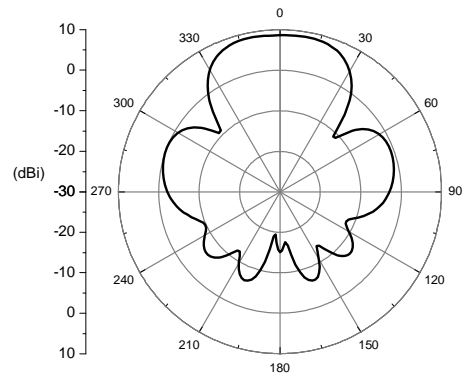
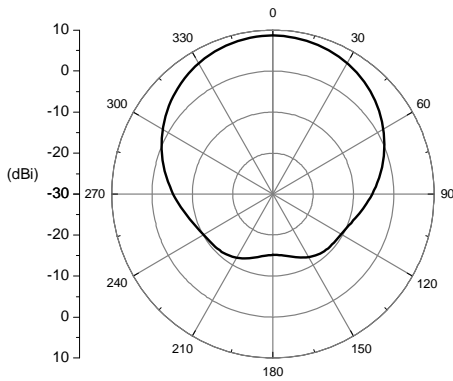


Fig. 14. Simulated poynting vector distribution in side view of two-element array with composite DGS and metal.



(a)



(b)

Fig. 15. Simulated gain patterns of the array with composite double U-shaped DGS and metal in Fig. 14; (a) in  $E$ -plane, (b) in  $H$ -plane.

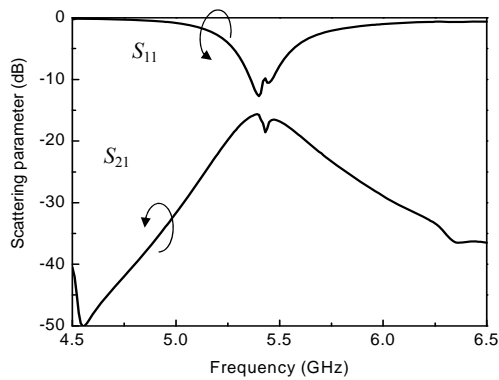


Fig. 16. Simulated input matching ( $S_{11}$ ) and mutual coupling ( $S_{21}$ ) of the two patches in Fig. 14.

#### IV. SCAN BLINDNESS ELIMINATION IN MICROSTRIP PHASED ARRAY

The scan characteristic of the infinite microstrip phased array is calculated and discussed in this section. Figure 17 gives the sketch of the infinite phased array cell. In this array, the periods along the  $x$ - and  $z$ -axis are the same of  $37.1\text{mm}$  (near  $0.65\lambda_0$ ), and the composite DGSs and SRRs are arranged for the reduction of mutual coupling in  $E$ -plane. Based on the waveguide simulator method, the array characteristic can be extracted by analyzing one of the elements in the array [24].

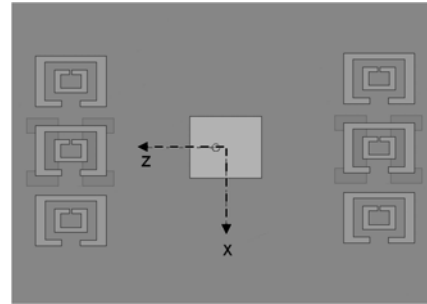
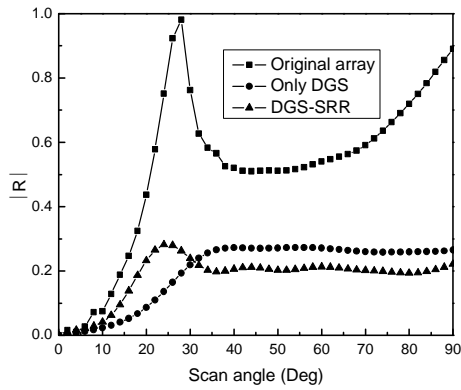


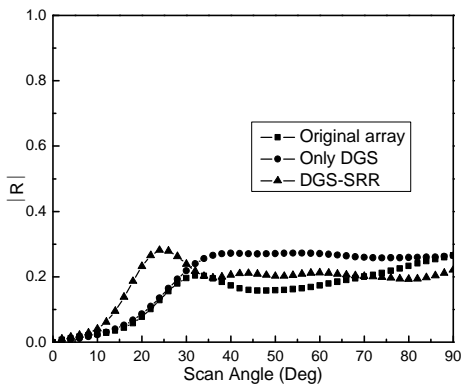
Fig. 17. Topological structure of an infinite phased array cell.

According to literature [24], Fig. 18 gives the calculated scan characteristics of the infinite microstrip phased array without DGSs, with only DGSs and with composite DGSs and SRRs at the resonant frequency of  $5.4\text{GHz}$ . These results indicate that, for the traditional phased array, scan blindness occurs at  $28^\circ$  in the  $E$ -plane and no scan blindness occurs in the  $H$ -plane. As depicted in literature [4], the scan blindness in the  $E$ -plane is well eliminated because of the usage of the DGSs. Meanwhile, the DGSs have a weak influence on the array reflection coefficient for the  $H$ -plane scan patterns. Just like the array with only DGSs, when loaded composite structures, the scan blindness in the  $E$ -plane array is eliminated as well and the array maintains excellent wide-angle impedance matching. Besides, its influence on scan performance in  $H$ -plane also counts for little.

The active element patterns for the centre element without DGSs, with only DGSs, and with composite structure are shown in Fig. 19, respectively. All of the patterns are plotted at the operation frequency ( $5.4\text{GHz}$ ). There are two significant nulls at  $28^\circ$  in the radiation pattern (in  $E$ -plane) for the array without DGSs in Fig. 20. The nulls are in accord with the blind spots obtained by the waveguide simulator method [5]. In addition, the radiation pattern of the array with the composite structures together with the array with only DGSs, is much smooth and has no apparent ripples in comparison with that of the traditional array. It is noted that, in contrast to the array with only DGSs, the array with composite structures also shows higher peak gain in front radiation and much lower gain in back radiation which results from inhibiting EM energy leaking through DGSs slots by SRRs.



(a)



(b)

Fig. 18. Scan characteristics of infinite microstrip array; (a) in *E*-plane, (b) in *H*-plane.

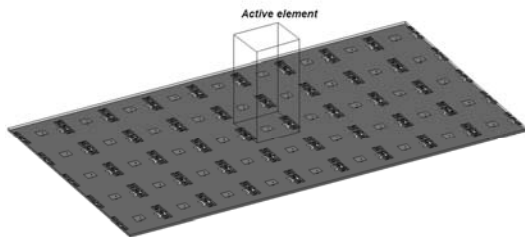
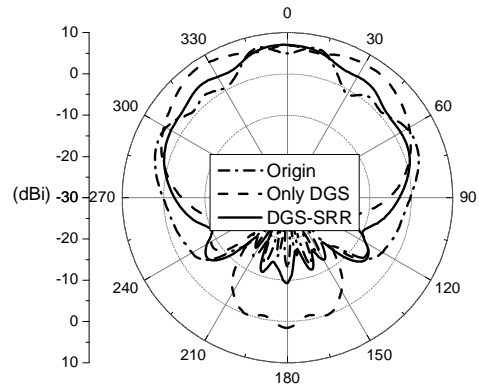
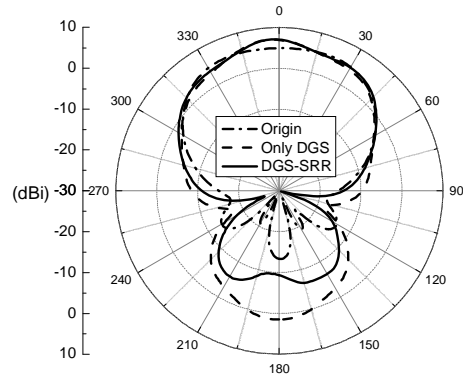


Fig. 19. Centre active element in the  $9 \times 5$  array.



(a)



(b)

Fig. 20. Normalized gain patterns of the centre active element against the scan angle in  $9 \times 5$  array in Fig.19; (a) in *E*-plane, (b) in *H*-plane.

### V. CONCLUSION

This paper concentrates on the application of the composite of DGSs and SRRs to eliminate the scan blindness of microstrip phased array by reducing the element mutual coupling. Two-element arrays without DGSs, with only DGSs, and with composite structures are simulated and measured, respectively. The results indicate that a mutual coupling decrease of 11 dB is well achieved at the operation frequency of the array, resulting from the composite structures. Moreover, compared with the array with only DGSs, 2dB gain improvement and 2.4dB side lobe suppression are also attained. Importantly, in our numerical investigation of three kinds of active patterns for center elements in  $9 \times 5$  element arrays, it

is found that the scan blindness in infinite microstrip phased array can be well eliminated by integrating proposed compact composite structures, in accordance with the simulation results in waveguide simulator. On account of its excellent isolation property and high mechanical strength, it is quite suitable for applying to high-performance array design, and promising for numerous other applications as well in the future.

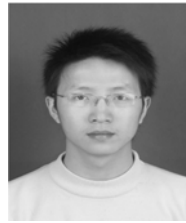
### ACKNOWLEDGMENT

The work was in part supported by the National Nature Science Foundation of China (Grant No. 60872034, 60971029), in part by the Natural Science Foundation of Educational Department of Sichuan Province, China (Grant No. 09ZA053), in part by the New-century Talent program of the Education Department of China (Grant No. NCET070154), and in part by the Aviation Science foundation (Grant No. 20090180007).

### REFERENCES

1. Y. Fu and N. Yuan, "Elimination of Scan Blindness in Phased Array of Microstrip Patches using Electromagnetic Bandgap Materials," *IEEE Antennas and Wireless Propag. Lett.*, vol. 3, pp. 63-65, 2004.
2. L. Zhang, J. A. Castaneda, and N. G. Alexopoulos, "Scan Blindness Free Phased Array Design using PBG Materials," *IEEE Trans. Antennas Propag.*, vol. 52, pp. 2000-2007, 2004.
3. B. Wu, H. Chen, J. A. Kong, and T. M. Grzegorzczak, "Surface Wave Suppression in Antenna Systems using Magnetic Metamaterial," *J. Appl. Phys.*, vol. 101, pp. 112913 (1-4), 2007.
4. K. Bull, H. Mosallaei, and K. Sarabandi, "Metamaterial Insulator Enabled Superdirective Array," *IEEE Trans. Antennas Propag.*, vol. 55, pp. 1047-1085, 2007.
5. D. -B. Hou, S. Xiao, B. -Z. Wang, L. Jiang, J. Wang, and W. Hong, "Elimination of Scan Blindness with Compact Defected Ground Structures in Microstrip Phased Array," *IET Microw. Antennas Propag.*, vol. 3, pp. 269-275, 2009.
6. D. Ahn, J.-S. Park, C.-S. Kim, J. Kim, Y. Qian, and T. Itoh, "A Design of the Low-Pass Filter using the Novel Microstrip Defected Ground Structure," *IEEE Trans. Microw. Theory Tech.*, vol. 49, pp. 86-93, 2001.
7. B. D. Braaten, R. P. Scheeler, M. Reich, R. M. Nelson, C. Bauer-Reich, J. Glower, and G. J. Owen, "Compact Metamaterial-Based UHF RFID Antennas: Deformed Omega and Split-Ring Resonator Structures," *Applied Computational Electromagnetic Society (ACES) Journal*, vol. 25, no. 6, pp. 530-542, Jun. 2010.
8. M. R. I. Faruque, M. T. Islam, and N. Misran, "Evaluation of EM Absorption in Human Head with Metamaterial Attachment," *Applied Computational Electromagnetic Society (ACES) Journal*, vol. 25, no. 12, pp. 1097-1107, Dec. 2010.
9. M.-C. Tang, S. Xiao, T. Deng, Y. Bai, J. Guan, and B.-Z. Wang, "Study of Miniaturized Electric Resonance Metamaterial," *Acta Physica Sinica*, vol. 59, no. 7, pp. 4715-4719, Jul. 2010.
10. M.-C. Tang, S. Xiao, J. Guan, Y. Bai, S. Gao, and B. -Z. Wang, "Composite Metamaterial Enabled Excellent Performance of Microstrip Antenna Array," *Chinese Physics B*, vol. 19, pp. 074214(1-5), Jul. 2010.
11. M.-C. Tang, S. Xiao, T. Deng, D. Wang, J. Guan, B. -Z. Wang, and G. Ge "Compact UWB Antenna with Multiple Band-Notches for WiMAX and WLAN," *IEEE Trans. Antennas Propag.*, vol. 59, no. 4, pp. 1372-1376, Apr. 2011
12. N. Katsarakis, T. Koschny, and M. Kafesaki, "Electric Coupling to the Magnetic Resonance of Split Ring Resonators," *Appl. Phys. Lett.*, vol. 84, pp. 2943-2945, 2004.
13. D. R. Smith, W. J. Padilla, D. C. Vier, S. C. Nemat-Nasser, and S. Schultz, "Composite Medium with Simultaneously Negative Permeability and Permittivity," *Phys. Rev. Lett.*, vol. 84, pp. 4184-4187, 2000.
14. J. D. Baena, J. Bonache, F. Martín, R. M. Sillero, F. Falcone, T. Lopetegui, M. A. G. Laso, J. García-García, I. Gil, M. F. Portillo, and M. Sorolla, "Equivalent-Circuit Models for Split-Ring Resonators and Complementary Split-Ring Resonators Coupled to Planar Transmission Lines," *IEEE Trans. Microwave Theory Tech.*, vol. 53, pp. 1451-1461, 2005.
15. D. R. Smith, J. Gollub, J. J. Mock, W. J. Padilla, and D. Schurig, "Calculation and Measurement of Bianisotropy in a Split Ring Resonator

- Metamaterial,” *J. Appl. Phys.*, vol. 100, pp. 024507(1-9), 2006.
16. P. Gay-Balmaz and O. J. F. Martina, “Electromagnetic Resonances in Individual and Coupled Split-Ring Resonators,” *J. Appl. Phys.*, vol. 92, pp. 2929-2936, 2002.
  17. T. Koschny, M. Kafesaki, E. N. Economou, and C. M. Soukoulis, “Effective Medium Theory of Left-Handed Materials,” *Phys. Rev. Lett.*, vol. 93, pp. 107402(1-4), 2004.
  18. R. W. Ziolkowski, “Design, Fabrication, and Testing of Double Negative Metamaterials,” *IEEE Trans. Antennas Propag.*, vol. 51, pp.1516-1528, 2003
  19. Y. X. Guo, K. M. Luk, and K. W. Leung, “Mutual Coupling Between Millimeter Wave Dielectric Resonator Antennas,” *IEEE Trans. Microw. Theory Tech.*, vol. 47, pp. 2164-2166, 1999.
  20. F. Yang and Y. Rahmat-Samii, “Microstrip Antennas Integrated with Electromagnetic Band-Gap (EBG) Structures: A Low Mutual Coupling Design for Array Applications,” *IEEE Trans. Antennas Propag.*, vol. 51, no. 10, pp. 2936-2945, 2003.
  21. A. H. Mohammadian, N. M. Martin, and D. W. Griffin, “A Theoretical and Experimental Study of Mutual Coupling in Microstrip Antenna Arrays,” *IEEE Trans. Antennas Propag.*, vol. 37, pp.1217-1223, 1989.
  22. R. P. Jedlicka, M. T. Poe, and K. R. Carver, “Measured Mutual Coupling Between Microstrip Antennas,” *IEEE Trans. Antennas Propag.*, vol. 29, pp. 147-149, 1981.
  23. K. Buell, H. Mosallaei, and K. Sarabandi, “A Substrate for Small Patch Antennas Providing Tunable Miniaturization Factors,” *IEEE Trans. Microw. Theory Tech.*, vol. 54, pp. 135-146, 2006.
  24. D. M. Pozar “Analysis of an Infinite Phased Array of Aperture Coupled Microstrip Patches,” *IEEE Trans. Antennas Propag.*, vol. 37, pp. 418-425, 1989.



**Ming-Chun Tang** received the B.S. degree in Physics from the Neijiang Normal University, Neijiang, China, in 2005. He is currently working toward the Ph.D. degree in Radio Physics at University of Electronic Science

and Technology of China (UESTC) from 2007. His research interest includes miniature antenna, RF circuit, metamaterial design, and its application. He has authored or coauthored more than 30 international referred journal and conference papers. He was a recipient of the Best Student Paper Award in 2010 International Symposium on Signals, Systems and Electronics (ISSSE2010). He serves as reviewers for the Journals *IEEE Antennas and Wireless Propagation Letters* and *IEEE Antennas and Propagation Magazine*.



**Shaoqiu Xiao** received the Ph.D. degree in Electromagnetic field and Microwave Engineering from the University of Electronic Science and Technology of China (UESTC), Chengdu, China, in 2003. From January 2004 to June 2004, he joined UESTC as an assistant professor. From July 2004 to March 2006, he worked for the Wireless Communications Laboratory, National Institute of Information and Communications Technology of Japan (NICT), Singapore, as a researcher with the focus on the planar antenna and smart antenna design and optimization. From July 2006 to June 2010, he worked for UESTC as an associate professor and now he is working for UESTC as a professor. His current research interests include planar antenna and array, microwave passive circuits and electromagnetic in ultrawide band communication. He has authored/coauthored more than 100 technical journals, conference papers, books, and book chapters.



**Chang-Jin Li** received the B.S. degree in Physics from the Sichuan Normal University, Sichuan, China, in 1989, and the master's degree in Pedagogics from the Sichuan Normal University, Sichuan, China, in 2004, respectively. His research interest includes laser characterization, propagation and transformation, resonator technology, and physics.



**Chaolei Wei** was born in Shandong Province, China, in 1981. He received the B.S. degree in Physics from the Liaocheng University, Liaocheng, Shandong, China in 2006, and the M.D. degree in Nuclear Energy Engineering from the Insititute of Southwest Physics, Chengdu in 2009, respectively, and is currently working toward the Ph.D. degree in Electrical Engineering at University of Electronic Science and Technology of China (UESTC). His research interests include microwave planar filters, microwave and millimeter-wave circuits, and systems design.



**Bingzhong Wang** received the Ph.D. degree in Electrical Engineering from the University of Electronic Science and Technology of China (UESTC), Chengdu, China, in 1988. He joined the UESTC in 1984 and is currently a Professor there. He has been a Visiting Scholar at the University of Wisconsin-Milwaukee, a Research Fellow at the City University of Hong Kong, and a Visiting Professor in the Electromagnetic Communication Laboratory, Pennsylvania State University, University Park. His current research interests are in the areas of computational electromagnetics, antenna theory and technique, electromagnetic compatibility analysis, and computer-aided design for passive microwave integrated circuits.